

FlyMirage: A Fully Automated Generation Pipeline for Diverse and Scalable UAV Flight Data via Generative World Model

Jinhan Li^{1,2,*}, Xijie Huang^{1,2,*}, Zhaoqi Wang², Yijin Wang^{1,2}, Weiqi Ge²,
Qiyi He², Mo Zhu^{1,2}, Fei Gao^{1,2,†}, Yuze Wu^{1,2,†} and Xin Zhou^{2,†}



Fig. 1: **FlyMirage**. It uses LLM-designed scene specifications, generative world model, automated scene annotation, and UAV-feasible trajectory planning to produce scalable, diverse, and photorealistic aerial VLN data.

Abstract—In the field of Vision-Language Navigation (VLN), aerial datasets remain limited in their ability to combine scale, diversity, and realism, often relying on either costly real-world scenes or visually limited simulations. To address these challenges, we introduce FlyMirage, a highly scalable and fully automated data generation pipeline for aerial VLN. Our approach leverages large language models (LLM) as an environment designer to promote scene diversity, paired with a generative world model that instantiates these designs into high-fidelity 3D Gaussian Splatting (3DGS) scenes. To substantially reduce human labor and ensure the feasibility of flight data, FlyMirage automates scene exploration and semantic information acquisition, and further integrates a dynamically feasible planner for uncrewed aerial vehicle (UAV) trajectory generation. Utilizing this toolchain, we generate a large-scale, diverse, and photorealistic aerial VLN dataset, with dynamically feasible flying trajectories, designed to support the development of next-generation embodied navigation models.

I. INTRODUCTION

Scaling high-quality robotics data has emerged as a promising pathway for advancing model capabilities in embodied artificial intelligence, mirroring the role of data scale in other domains [1]. For example, models such as Gen-1

[2], trained on approximately half a million hours of real-world data, demonstrate strong generalization capabilities, highlighting the importance of large-scale data. This naturally raises the question of whether similar scaling laws could apply to aerial Vision-Language Navigation (VLN), where available datasets remain relatively underexplored. To better understand existing aerial VLN data sources, these can be categorized into two types: real-world and simulated data.

Real-world navigation data is costly to collect and difficult to scale, requiring experienced human operators. For example, UAV-Flow [3] collected 100 hours of pilot-operated flight data, but its environmental coverage remains limited to university campuses. In contrast, simulated data enables a safer, cheaper and more scalable approach. Simulated data refers to data collected in digital environments, including real-world reconstructions [4], [5], [6], [7], and scenes built with virtual 3D assets. Within these simulations, prior efforts such as OpenFly [8] attempt to automate trajectory generation with A* [9] in 18 pre-constructed scenes, but their scalability remains bounded by the availability of high-quality predefined environments. Despite this progress, can existing data pipelines provide data that is realistic and diverse enough to reveal the true effects of the scaling law? We argue that current real-world and simulated data pipelines still face three key limitations:

*Equal Contributions

¹State Key Laboratory of Industrial Control Technology, Zhejiang University, Hangzhou 310027, China.

²Differential Robotics, Hangzhou 311121, China.

[†]Corresponding authors: Fei Gao, Yuze Wu and Xin Zhou.

- 1) **Limited visual and geometric fidelity.** Asset-based virtual environments suffer from simplified textures, materials, and lighting, increasing the visual sim-to-real gap.
- 2) **Insufficient data diversity and scale.** Achieving scalable diversity of high-quality scenes remains difficult for both real-world and simulation pipelines, as they often require human intervention in scene construction, scene annotation or trajectory collection.
- 3) **Dynamics-unaware trajectory generation.** Although prior attempts have used search-based algorithms for automated trajectory generation, they ignore robot dynamics and can produce trajectories that are unnatural or infeasible for real-world UAV deployment.

Recent advances in generative world models offer a compelling opportunity to overcome these limitations. In particular, foundation models like Marble [10] can generate explorable 3D worlds with coherent spatial structures from text or image prompts. This capability opens up a promising avenue for rethinking aerial VLN data generation: instead of relying on data collected in real-world environments or manually constructed virtual spaces, we can automatically generate realistic, explorable worlds and collect navigation data within them.

Building on this capability, we propose a scalable and fully automated pipeline for generating aerial VLN data (Fig. 1). To enrich scene diversity, we leverage large language models (LLM) as a navigation environment designer that generates diverse structured scene specifications, which are then instantiated by the generative world model into photorealistic, explorable 3D worlds. This design enables a dataset to cover a broad spectrum of environments, ranging from common indoor and outdoor scenes to hazardous, access-restricted, and hard-to-reconstruct spaces such as radiation-risk areas or chemical facilities. To reduce the visual sim-to-real gap, we use Marble 1.1 Plus as the generative world model, following a text&image-to-world paradigm to create high-fidelity 3D Gaussian Splatting (3DGS) [11] scenes. To minimize human involvement, we automate camera exploration and scene annotation. We further develop an automatic aerial navigation target-generation system based on the resulting scene annotations, and integrate a UAV-specific dynamically feasible trajectory planner for trajectory generation. We denote this fully automated pipeline as **FlyMirage**: with a single command, it can continuously generate a virtually unbounded collection of diverse scenes and corresponding navigation trajectories.

Therefore, we position FlyMirage as the next-generation tool of automated aerial VLN data collection. To validate its potential, we generate 500 distinct example scenes from indoor to outdoor and 50K navigation trajectories automatically. Comparing with existing VLN datasets, FlyMirage offers superior extensibility and observation fidelity, while also producing physically executable aerial trajectories. Moreover, the monetary and time costs of data generation are substantially lower: FlyMirage requires only Marble and a consumer-grade NVIDIA GPU to render RGB images

from 3DGS scenes, in contrast to the manual mesh creation required by InteriorGS [12] or the human-operated drone flights required in UAV-Flow [3] that cost approximately \$100 per hour.

We summarize our contributions as follows:

- 1) We introduce **FlyMirage**, a novel data source for aerial VLN with scalable diversity, powered by a generative world model and supported by a fully automated data collection pipeline.
- 2) We design an iterative scene annotation strategy based only on the 3DGS representation of the scene without any other prior information such as training images.
- 3) Using our toolchain, we generate and release a large-scale open dataset for the aerial VLN community.

II. RELATED WORK

A. Labor Intensive Dataset Collection

Vision-Language Navigation (VLN) tasks originated in ground robotics, which fundamentally require large-scale datasets to train navigation models. Early works primarily utilized graph-based maps, enabling discrete node sampling, coupled with manual data annotation [4][5].

In the context of UAV, higher degrees of freedom make automatic data collection significantly more challenging. To address this, several works have relied on manual data collection. For instance, UAV-Flow [3] amassed 30k episodes controlled by human operators in the real world. Other efforts have crowdsourced trajectories from humans flying drones within simulated environments, including CityNAV [13], AerialVLN [14], and AVDN [15]. Despite relying on manual trajectory generation, some works, such as OpenUAV [16], leverage large language models to automatically generate natural language annotations for these paths.

B. Automatic Dataset Collection

Significant efforts have also been directed toward automating trajectory generation, although such approaches often still require manual 3D scene construction. To facilitate this, SAGE-3D [7] handcrafted 1,000 3DGS scenes, introduced as InteriorGS [12]. Based on such constructed scenes, search-based planning algorithms has become a standard approach for automatically generating trajectories in both ground [6], [7] and aerial robotics [8]. Alternatively, approaches like Youtube-VLN [17] and Roomtour3D [18] bypass 3D representations entirely by repurposing existing room-tour videos. A major limitation of this video-based approach is its constraint to pre-existing viewpoints, often lacking movement along the z-axis, which is crucial for UAV navigation. While there are attempts to generate scaled 3D mesh scene representations [19], [20], these methods function primarily as mesh assemblers. Mesh-based scene representations are inherently more suited for Vision-Language-Action (VLA) manipulation tasks rather than navigation, and their relatively low fidelity has thus far precluded the collection of dedicated navigation datasets. While recent work [21] leverages video

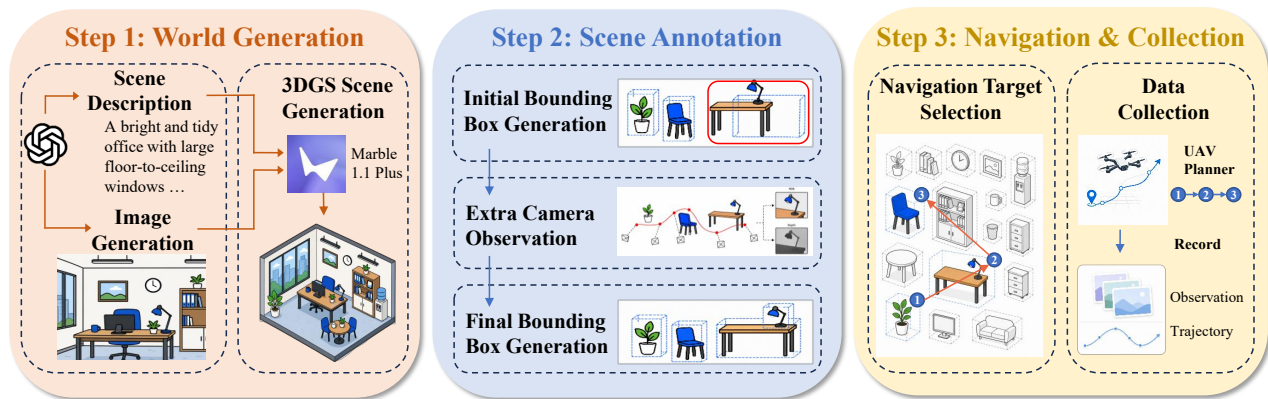


Fig. 2: **Overall Dataset Creation Pipeline of FlyMirage.** It consists of three stages: World Generation, Scene Annotation and Navigation & Collection.

world models to synthesize training data, it incurs a prohibitive computational cost, requiring approximately 81,000 NVIDIA L40 GPU hours to generate 240k samples.

III. PIPELINE FOR DATASET CREATION

As illustrated in Fig. 2, our pipeline automatically generates scalable UAV navigation datasets by transforming batch-produced scene descriptions into UAV trajectories for training navigation policies.

A. World Generation

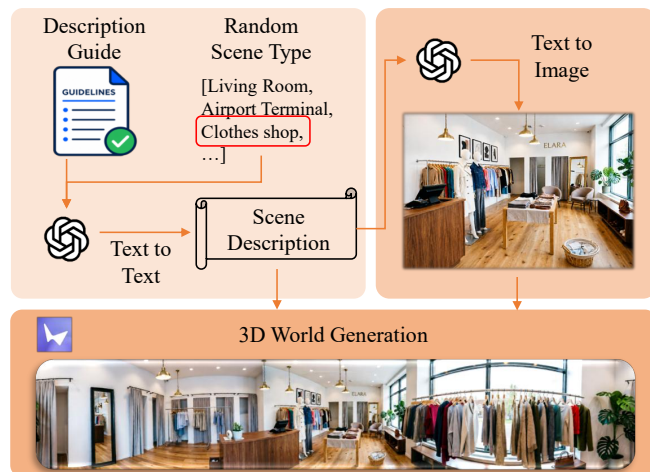


Fig. 3: **World Generation.** A description guide is paired with a randomly selected scene type to generate a detailed scene description and image, which are then used to create a 3DGS scene with Marble.

We organize common types of scenes into a hierarchical taxonomy of categories and subcategories. To generate a scene description, we first randomly select a subcategory within a broader category, and then prompt GPT-5.4 or Gemini 3.1 to describe a scene corresponding to that selected type. This two-step procedure is designed to mitigate the uneven sampling behavior we observed when prompting LLMs to generate random scene descriptions directly. In particular, direct prompting often led to a biased distribution

over scene types; for example, GPT-5.4 produced medical-related descriptions substantially more frequently than other common environments. By explicitly pre-selecting the scene type from a hierarchical taxonomy, we decouple the choice of scene category from the generative preferences of the language model. This allows us to maintain a more controlled and balanced distribution of scene types while still benefiting from the model’s ability to produce diverse, detailed, and naturalistic descriptions of common real-world spaces.

Given the resulting textual description, we next generate a corresponding image using GPT Images 2.0. This image generation step provides a visually grounded representation of the scene, complementing the language-only description with concrete spatial, appearance, and layout cues. Compared with a text description alone, the generated image can capture additional visual details such as object placement, material appearance, lighting conditions, color composition, and the overall spatial arrangement of the environment. We then use both the generated image and the original textual description as inputs to Marble 1.1 Plus to generate a 3DGS-based scene, as illustrated in Fig. 3.

B. Scene Annotation

Marble produces only a 3DGS scene representation, without training images or object-level semantic information. To obtain object-level annotation, we use Boxer [22] to perform open-vocabulary object detection and estimate 3D bounding boxes for the detected objects. Specifically, we use GSplat [23]-rendered RGB images and the corresponding estimated depth maps as inputs to Boxer. However, due to the limitation of the Boxer algorithm, the 3D bounding-box estimates become less accurate for objects that are far from the rendering viewpoint.

Thus, we use a simple iterative method to explore the scene as shown in Fig. 4. Since Marble follows a “prompt-to-panorama-to-world” pipeline, every generated scene has a center c . Since the immediate neighborhood of this point is typically object-free, we orbit the camera around it with radius $r_{\text{orb}} = 0.1$ m. For each yaw-pitch pair (ψ, θ) , with yaw ψ measured from $+y$, we define

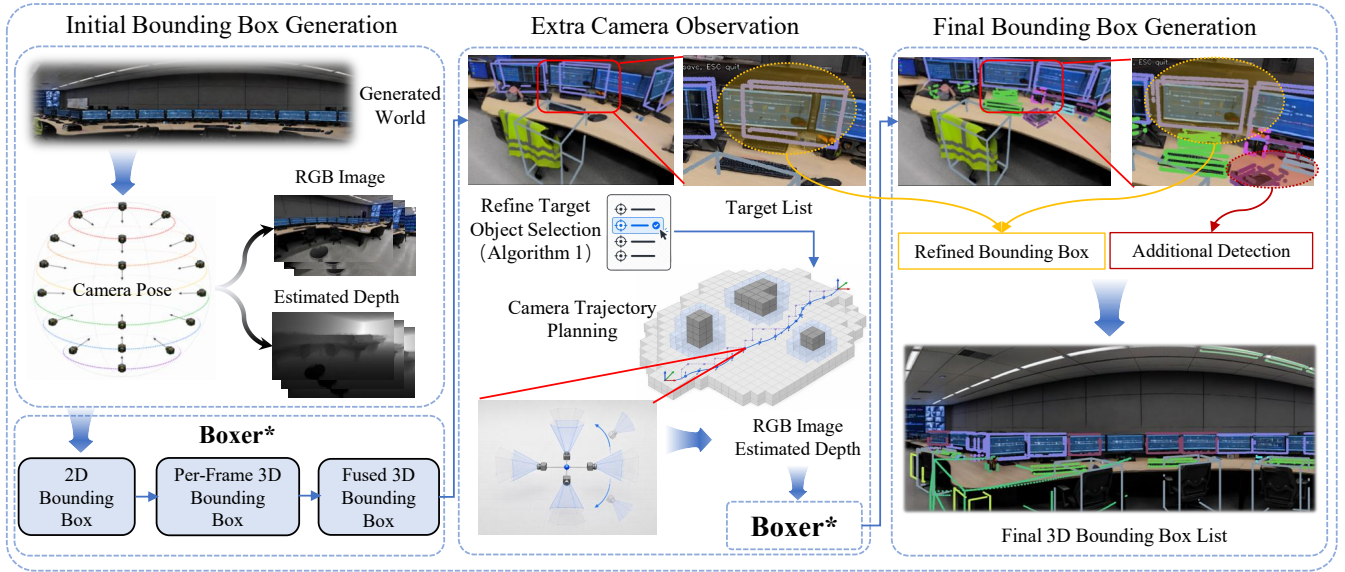


Fig. 4: **Scene Annotation.** An iterative algorithm is used to generate accurate bounding boxes for objects in generated scenes. (*Boxer [22] is a 3D bounding box estimation algorithm by Meta Reality Labs)

$$\mathbf{d}(\psi, \theta) = \begin{bmatrix} \sin \psi \cos \theta \\ \cos \psi \cos \theta \\ \sin \theta \end{bmatrix}, \quad \mathbf{p}(\psi, \theta) = \mathbf{c} - r_{\text{orb}} \mathbf{d}(\psi, \theta).$$

Each camera position $\mathbf{p}(\psi, \theta)$ is paired with the viewing direction $\mathbf{d}(\psi, \theta)$, orienting the camera to look through the world center \mathbf{c} . This inward-facing orbit keeps the camera within the empty central region and makes scene objects more likely to be observed through a small free-space buffer (the object-free sphere around \mathbf{c}). Camera viewpoints are sampled at multiple elevation angles over the viewing sphere, with a complete yaw sweep performed at each elevation, as illustrated by the camera pose visualization in Fig. 4.

Given these camera poses, we render RGB images and estimated depth maps and feed them to Boxer. We denote the returned 3D bounding boxes as the candidate set $\mathcal{O} = \{\mathbf{o}_i\}_{i=1}^N$. Due to limitations of Boxer, we define two distance thresholds, $0 < d_{\text{th1}} < d_{\text{th2}}$. Predicted bounding boxes for objects farther than d_{th2} are often substantially inaccurate and therefore require closer camera observation, whereas bounding boxes for objects with distances between d_{th1} and d_{th2} may be slightly inaccurate but remain within an acceptable range. Targets for extra camera observation are then selected from \mathcal{O} using a distance-aware procedure that promotes spatial diversity. Let N_t denote the maximum number of targets to be selected. For each candidate bounding box in \mathcal{O} with center \mathbf{x}_i , we compute its distance to the scene center as $d_i = \|\mathbf{x}_i - \mathbf{c}\|_2$.

As shown in Algorithm 1, starting from the farthest candidate, we greedily accept candidates with $d_i > d_{\text{th2}}$. After accepting a candidate, we discard nearby objects within d_{prune} where $d_{\text{prune}} = d_{\text{th1}}$, or whose azimuth with respect to \mathbf{c} differs by less than θ_{th} , to avoid selecting multiple targets that are too close or lie in the same direction. If no

candidate beyond d_{th2} is selected, we fall back to candidates with $d_i \in (d_{\text{th1}}, d_{\text{th2}}]$ and select the farthest one; if none exists, no extra camera observation is needed for the current scene.

Given a selected target, we plan a collision-checked 3D waypoint path toward the target using voxel-based A* search on an inflated occupancy grid with collision-aware Laplacian smoothing, yielding a dense camera trajectory of the scene: $\{\mathbf{q}_k\}_{k=1}^K$, where each $\mathbf{q}_k \in \mathbb{R}^3$ denotes a camera position along the path. At each position, the camera heading is aligned with a temporally smoothed estimate of the local path tangent. A four-view camera rig is placed at the same position, with different yaw offsets corresponding to front, left, right, and back views. Each camera position therefore produces four synchronized observations, providing near-panoramic coverage along the trajectory.

Using the extra camera observations together with the initial rotational observations, we rerun a modified Boxer framework. While the standard pipeline fuses per-frame 3D detections into a global map, we introduce a distance-based pruning constraint. By filtering out every Boxer 3D detection beyond a d_{th1} threshold from the camera optical center in each frame, we eliminate distant artifacts and ensure the fidelity of the final fused global bounding box map.

In our implementation, to ensure both data diversity and accurate bounding-box localization, we set $N_t = 5$, $\theta_{\text{th}} = 35^\circ$, $d_{\text{th1}} = 3.0$ m, and $d_{\text{th2}} = 4.0$ m.

C. Navigation & Collection

As shown in Fig. 5, the navigation and data collection process requires only two scene-level inputs: a semantic annotation file containing object labels with their corresponding 3D bounding boxes, and a 3D Gaussian Splatting representation. For each scene, we specify the number of target sets, N_s , and the number of targets per set, N_o . The

Algorithm 1 Distance-Aware Target Selection

Require: Candidate set $\mathcal{O} = \{\mathbf{o}_i\}_{i=1}^N$ with box centers $\{\mathbf{x}_i\}_{i=1}^N$, scene center \mathbf{c} , thresholds d_{th1} , d_{th2} , θ_{th} , maximum number of targets N_t

- 1: Compute $d_i \leftarrow \|\mathbf{x}_i - \mathbf{c}\|_2$ for each candidate \mathbf{o}_i
- 2: Sort \mathcal{O} in descending order by d_i
- 3: Initialize target set $\mathcal{T} \leftarrow \emptyset$
- 4: Initialize active candidate set $\mathcal{A} \leftarrow \mathcal{O}$
- 5: **for** each candidate $\mathbf{o}_i \in \mathcal{O}$ in sorted order **do**
- 6: **if** $\mathbf{o}_i \notin \mathcal{A}$ **then**
- 7: **continue**
- 8: **end if**
- 9: **if** $d_i \leq d_{th2}$ **then**
- 10: **continue**
- 11: **end if**
- 12: Add \mathbf{o}_i to \mathcal{T}
- 13: Set $d_{prune} = d_{th1}$
- 14: Remove from \mathcal{A} all remaining candidates \mathbf{o}_j that
 $\|\mathbf{x}_j - \mathbf{x}_i\|_2 < d_{prune}$ **or** $\Delta_{az}(i, j) < \theta_{th}$
- 15: **if** $|\mathcal{T}| = N_t$ **then**
- 16: **break**
- 17: **end if**
- 18: **end for**
- 19: **if** $\mathcal{T} = \emptyset$ **then**
- 20: Initialize set $\mathcal{Q} \leftarrow \{\mathbf{o}_i \in \mathcal{O} : d_{th1} < d_i \leq d_{th2}\}$
- 21: **if** $\mathcal{Q} \neq \emptyset$ **then**
- 22: $\mathcal{T} \leftarrow \{\arg \max_{\mathbf{o}_i \in \mathcal{Q}} d_i\}$
- 23: **end if**
- 24: **end if**
- 25: **return** \mathcal{T}

program then generates the target sets sequentially. Within each set, targets are selected one at a time until N_o valid targets have been obtained.

We use the scene annotation file as the list of candidate targets. Each candidate must pass several checks before being accepted and counted toward N_o . The eligibility criteria are as follows:

- **Position Validation:** The current drone position must not lie inside the candidate object’s 3D bounding box.
- **Visibility Check:** A candidate object is accepted only if it is visible from the drone’s current position. Visibility is checked by casting a ray from the drone toward the object’s bounding box. If any occupied point lies within a cylindrical region around the ray before the ray reaches the object, the object is treated as occluded and rejected.

After the candidate passes first two checks, we compute a candidate target point around the candidate object, with a slight offset toward the starting position to ensure that the drone ends up in free space.

- **Waypoint Safety:** The algorithm evaluates a small region around the candidate target point. The candidate is rejected if any occupied point falls within this safety

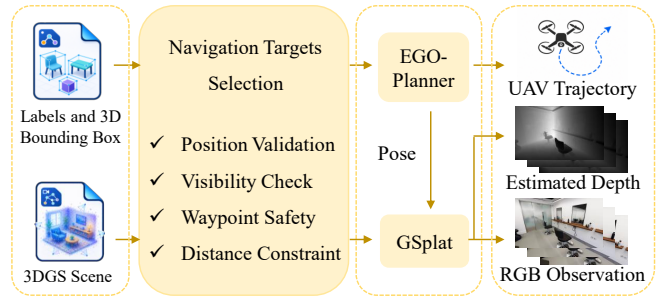


Fig. 5: **Navigation & Collection.** An automated pipeline to determine the trajectory goals and deploy EGO-Planner to fly the drone between them.

region.

- **Distance Constraint:** The travel distance from the current position to the candidate target point must lie within the range of 2.0 m to 10.0 m.

Candidates that satisfy all conditions are accepted into the target set and used to update the drone position for selecting the next target. After all N_s sets are generated, the resulting target points are written to task files and passed to EGO-Planner [24], a dynamically feasible UAV planner validated in extensive simulation and real-world experiments, for on-line trajectory planning. Along each planned trajectory, RGB observations and estimated depth maps are rendered from the 3D Gaussian Splatting representation using GSplat and recorded together with the corresponding drone trajectory.

Within the collected flight data, RGB images from each trajectory are sampled at 30-frame intervals. The sampled frames are then concatenated and used to query Qwen-3.5-Flash [27] for automated visual quality assessment, filtering out trajectories with severe rendering artifacts, poor visibility, or unclear flight intent. Only trajectories that are validated as high-quality are archived in FlyMirage.

For each valid trajectory, we further query Qwen-3.5-Flash to generate up to three prompt variants, each emphasizing a different aspect of the target object:

- **Original Object-Centered:** Prompts that directly refer to the target object, e.g., “Find the bookshelf.”
- **Relative-Positioned:** Prompts that describe the target object through its spatial relationship to nearby objects, e.g., “Go to the chair next to the bookshelf.”
- **Appearance-Centered:** Prompts that identify the target object based on visual attributes such as color, shape, or material, e.g., “Navigate to the green sofa.”

By collecting multiple prompt formulations for the same trajectory, FlyMirage supports tasks under diverse referring-expression styles.

IV. DATASET ANALYSIS

Our dataset contains 500 3DGS scenes spanning six categories as shown in Fig. 6: transportation spaces; workplaces and offices; commercial and retail spaces; industrial and utility facilities; leisure and hospitality venues; homes and residential spaces. Existing aerial VLN datasets are often



Fig. 6: **Dataset Statistics**. Top is the distribution of scene categories. Bottom left is object count distribution in generated scenes. Bottom right is trajectory statistics & example trajectory.

TABLE I: Trajectory Datasets Comparison

Dataset	N_{traj}	Action Space	N_{scenes}	Scene Environment	Traj Generation	Traj Annotation	Kinematics	Scene/Traj Extensibility
R2R[4]	7189	Node-based	90	Matterport3D	Sampling from Nodes	Human Annotation	No	Manual Scan
RxR[5]	13992	Node-based	90	Matterport3D	Sampling from Nodes	Human Annotation	No	Manual Scan
VLN-CE[6]	4475	2 DoF	90	Matterport3D	A* between R2R Path Nodes	Adapted from R2R	No	Manual Scan/Auto Record
LHPR-VLN[25]	3260	2 DoF	216	HM3D	D* Lite-based	LLM-based	No	Manual Scan/Auto Record
SAGE-3D[7]	100K+*	2 DoF	1000	3DGS	A*	LLM-based	No	Manual Scan/Auto Record
AVDN[15]	6269	3 DoF	-	xView	Human Control	Human Annotation	No	Manual Record
AerialVLN[14]	8446	4 DoF	25	AirSim + UE	Human Control	Human Annotation	No	Manual Scan/Record
CityNav[13]	32637	4 DoF	34	SensatUrban	Human Control	Pre-existed Dataset (City Refer)	No	Manual Scan/Record
OpenUAV[16]	12149	6 DoF	22	AirSim + UE	Human Control	LLM-based	Yes	Manual Scan/Record
OpenFly[8]	100K	4 DoF	18	AirSim, GTA5, 3DGS, GE	A*	LLM-based	No	Manual Scan/Auto Record
UAV-Flow[3]	40801	6 DoF	-	Real World, UnrealCV	Human Control	Human Annotation + LLM	Yes	Manual Scan/Record
IndoorUAV[26]	34925	4 DoF	1075	Mp3D, Gibson, HM3D, Replica	Human Control	LLM-based	No	Manual Scan/Record
FlyMirage	50K	6 DoF	500	3DGS	Dynamically Feasible UAV Planner	LLM-based	Yes	Fully Automated

*: Despite SAGE-3D provides 2 million instruction-trajectory pairs, each trajectory is associated with 15-20 prompts and the total trajectory number is approximately 100K+

collected in predominantly residential scenes. For example, HM3D [28] used by IndoorUAV is primarily home-focused, and approximately 75% of scenes in SAGE-3D are residential. In contrast, FlyMirage provides a more balanced and diverse distribution of scene types as shown in Fig. 6, making it better suited for training models that can generalize across a wider range of real-world environments beyond residential spaces.

Across these scenes, more than 5,000 unique object labels are automatically identified, along with associated bounding boxes for each object instance. A typical scene in this dataset contains 60–100 object instances, providing sufficient semantic context for downstream navigation. Although other datasets, such as InteriorGS, also contain many object instances, a large portion of these instances are repetitive, resulting in only around 700 unique object categories across all scenes of the dataset.

Using this data, we collect around 50,000 navigation tra-

jectories, primarily between object-centric waypoints. Each trajectory is generated using EGO-Planner, providing dynamically feasible motion information that accounts for kinematic constraints, in contrast to prior datasets that rely on A* planning or discrete action spaces. As shown in Table I, ours is the first automated aerial trajectory-generation pipeline to produce true 6-DoF trajectories, a capability previously available only through human-controlled data collection.

The mean and median trajectory lengths are 4.33 m and 4.06 m. As we also record up to five navigation tasks within a continuous run, trajectories can be composed into long-horizon tasks of up to approximately four to five times the typical path length, or around 20 m. As a result, our dataset supports training and evaluation for both short- and long-horizon aerial VLN tasks. In addition, through our LLM-based prompt diversification process, each trajectory is associated with 2–3 prompts, enabling more varied language

supervision for navigation.

Moreover, the monetary cost and human effort required to generate our dataset are extremely low. The total API cost, including Marble and all LLM calls, is approximately \$2 per scene, and batch rendering with GSplat requires only a consumer-grade NVIDIA RTX 4070 GPU. From initialization to trajectory collection, the full pipeline takes about one hour per scene and can be parallelized across batches. In comparison, commonly used simulation-reconstruction pipelines such as HM3D require a dedicated Matterport Pro2 sensor, which costs approximately \$3,000, to scan an environment, while SAGE-3D requires manual scene design for each individual scene. Therefore, prior methods often involve substantial human effort, whereas our method operates automatically without manual intervention.

V. CONCLUSION & FUTURE WORK

In this paper, we present FlyMirage, an automated pipeline that bridges the gap between scale and realism in aerial Vision-Language Navigation. With it, we produce a dataset featuring 5,000+ unique object labels and 50,000 dynamically feasible UAV trajectories. It provides photorealistic images and 6-DoF trajectory data suitable for both short- and long-horizon navigation, which could be useful for aerial VLA/VLN [29] and action world model for aerial navigation [30]. In the future, this scalable toolchain and dataset could serve as a robust foundation for training next-generation embodied AI agents, including general aerial navigation models capable of operating effectively across diverse and complex real-world scenes.

REFERENCES

- [1] J. Kaplan, S. McCandlish, T. Henighan, T. B. Brown, B. Chess, R. Child, S. Gray, A. Radford, J. Wu, and D. Amodei, "Scaling laws for neural language models," *arXiv preprint arXiv:2001.08361*, 2020.
- [2] G. A. Team, "Gen-1: Scaling embodied foundation models to mastery," *Generalist AI Blog*, 2026, <https://generalistai.com/blog/apr-02-2026-GEN-1>.
- [3] X. Wang, D. Yang, Y. Liao, W. Zheng, wenjun wu, B. Dai, H. Li, and S. Liu, "Uav-flow colosso: A real-world benchmark for flying-on-a-word uav imitation learning," 2025. [Online]. Available: <https://arxiv.org/abs/2505.15725>
- [4] P. Anderson, Q. Wu, D. Teney, J. Bruce, M. Johnson, N. Sünderhauf, I. Reid, S. Gould, and A. van den Hengel, "Vision-and-language navigation: Interpreting visually-grounded navigation instructions in real environments," in *Proceedings of the IEEE Conference on Computer Vision and Pattern Recognition (CVPR)*, 2018.
- [5] A. Ku, P. Anderson, R. Patel, E. Ie, and J. Baldridge, "Room-Across-Room: Multilingual vision-and-language navigation with dense spatiotemporal grounding," in *Conference on Empirical Methods for Natural Language Processing (EMNLP)*, 2020.
- [6] J. Krantz, E. Wijmans, A. Majumdar, D. Batra, and S. Lee, "Beyond the nav-graph: Vision and language navigation in continuous environments," in *European Conference on Computer Vision (ECCV)*, 2020.
- [7] B. Miao, R. Wei, Z. Ge, X. sun, S. Gao, J. Zhu, R. Wang, S. Tang, J. Xiao, R. Tang, and J. Li, "Towards physically executable 3d gaussian for embodied navigation," 2025. [Online]. Available: <https://arxiv.org/abs/2510.21307>
- [8] Y. Gao, C. Li, Z. You, J. Liu, Z. Li, P. Chen, Q. Chen, Z. Tang, L. Wang, P. Yang, Y. Tang, Y. Tang, S. Liang, S. Zhu, Z. Xiong, Y. Su, X. Ye, J. Li, Y. Ding, D. Wang, Z. Wang, B. Zhao, and X. Li, "Openfly: A comprehensive platform for aerial vision-language navigation," *CoRR*, vol. abs/2502.18041, 2025.
- [9] P. E. Hart, N. J. Nilsson, and B. Raphael, "A formal basis for the heuristic determination of minimum cost paths," *IEEE Trans. Syst. Sci. Cybern.*, vol. 4, pp. 100–107, 1968. [Online]. Available: <https://api.semanticscholar.org/CorpusID:206799161>
- [10] World Labs, "Marble models," <https://docs.worldlabs.ai/marble/models>, 2026, accessed: 2026-05-09.
- [11] B. Kerbl, G. Kopanas, T. Leimkühler, and G. Drettakis, "3d gaussian splatting for real-time radiance field rendering," *ACM Transactions on Graphics*, vol. 42, no. 4, July 2023. [Online]. Available: <https://repo-sam.inria.fr/fungraph/3d-gaussian-splatting/>
- [12] M. T. I. SpatialVerse Research Team, "InteriorGS: A 3d gaussian splatting dataset of semantically labeled indoor scenes," <https://huggingface.co/datasets/spatialverse/InteriorGS>, 2025.
- [13] J. Lee, T. Miyaniishi, S. Kurita, K. Sakamoto, D. Azuma, Y. Matsuo, and N. Inoue, "Citynav: Language-goal aerial navigation dataset with geographic information," 2024.
- [14] S. Liu, H. Zhang, Y. Qi, P. Wang, Y. Zhang, and Q. Wu, "Aerialvln: Vision-and-language navigation for uavs," in *International Conference on Computer Vision (ICCV)*, 2023.
- [15] Y. Fan, W. Chen, T. Jiang, C. Zhou, Y. Zhang, and X. E. Wang, "Aerial vision-and-dialog navigation," in *Findings of the Association for Computational Linguistics: ACL 2023*. Toronto, Canada: Association for Computational Linguistics, Jul. 2023, pp. 3043–3061. [Online]. Available: <https://aclanthology.org/2023.findings-acl.190>
- [16] X. Wang, D. Yang, Z. Wang, H. Kwan, J. Chen, W. Wu, H. Li, Y. Liao, and S. Liu, "Towards realistic uav vision-language navigation: Platform, benchmark, and methodology," 2024. [Online]. Available: <https://arxiv.org/abs/2410.07087>
- [17] K. Lin, P. Chen, D. Huang, T. H. Li, M. Tan, and C. Gan, "Learning vision-and-language navigation from youtube videos?" *arXiv preprint arXiv:2307.11984*, 2023.
- [18] M. Han, L. Ma, K. Zhumakhanova, E. Radionova, J. Zhang, X. Chang, X. Liang, and I. Laptev, "Roomtour3d: Geometry-aware video-instruction tuning for embodied navigation," *arXiv preprint arXiv:2412.08591*, 2023.
- [19] Y. Yang, F.-Y. Sun, L. Weihs, E. VanderBilt, A. Herrasti, W. Han, J. Wu, N. Haber, R. Krishna, L. Liu, C. Callison-Burch, M. Yatskar, A. Kembhavi, and C. Clark, "Holodeck: Language guided generation of 3d embodied ai environments," in *Proceedings of the IEEE/CVF Conference on Computer Vision and Pattern Recognition (CVPR)*, June 2024, pp. 16 227–16 237.
- [20] Y. Yang, B. Jia, S. Zhang, and S. Huang, "Sceneweaver: All-in-one 3d scene synthesis with an extensible and self-reflective agent," in *Advances in Neural Information Processing Systems (NeurIPS)*, 2025.
- [21] J. Jang, S. Ye, Z. Lin, J. Xiang, J. Bjorck, Y. Fang, F. Hu, S. Huang, K. Kundalia, Y.-C. Lin *et al.*, "Dreamgen: Unlocking generalization in robot learning through video world models," *arXiv preprint arXiv:2505.12705*, 2025.
- [22] D. DeTone, T. Shen, F. Zhang, L. Ma, J. Straub, R. Newcombe, and J. Engel, "Boxer: Robust lifting of open-world 2d bounding boxes to 3d," 2026.
- [23] V. Ye, R. Li, J. Kerr, M. Turkulainen, B. Yi, Z. Pan, O. Seiskari, J. Ye, J. Hu, M. Tancik, and A. Kanazawa, "gsplat: An open-source library for gaussian splatting," *Journal of Machine Learning Research*, vol. 26, no. 34, pp. 1–17, 2025.
- [24] X. Zhou, Z. Wang, H. Ye, C. Xu, and F. Gao, "Ego-planner: An esdf-free gradient-based local planner for quadrotors," *IEEE Robotics and Automation Letters*, vol. 6, no. 2, pp. 478–485, 2021.
- [25] X. Song, W. Chen, Y. Liu, W. Chen, G. Li, and L. Lin, "Towards long-horizon vision-language navigation: Platform, benchmark and method," in *Proceedings of the IEEE/CVF Conference on Computer Vision and Pattern Recognition*, 2025.
- [26] X. Liu, Y. Liu, H. Qiu, Y. Qirong, and Z. Lian, "Indooruav: Benchmarking vision-language uav navigation in continuous indoor environments," in *Proceedings of the AAAI Conference on Artificial Intelligence*, vol. 40, no. 28, 2026, pp. 23 864–23 872.
- [27] Qwen Team, "Qwen3.5: Towards native multimodal agents," February 2026. [Online]. Available: <https://qwen.ai/blog?id=qwen3.5>
- [28] S. K. Ramakrishnan, A. Gokaslan, E. Wijmans, O. Maksymets, A. Clegg, J. M. Turner, E. Undersander, W. Galuba, A. Westbury, A. X. Chang, M. Savva, Y. Zhao, and D. Batra, "Habitat-matterport 3d dataset (HM3d): 1000 large-scale 3d environments for embodied AI," in *Thirty-fifth Conference on Neural Information Processing Systems Datasets and Benchmarks Track*, 2021. [Online]. Available: <https://arxiv.org/abs/2109.08238>

- [29] Y. Wu, M. Zhu, X. Li, Y. Du, Y. Fan, W. Li, Z. Han, X. Zhou, and F. Gao, "Vla-an: An efficient and onboard vision-language-action framework for aerial navigation in complex environments," 2025. [Online]. Available: <https://arxiv.org/abs/2512.15258>
- [30] X. Huang, W. Gai, T. Wu, C. Wang, Z. Liu, X. Zhou, Y. Wu, and F. Gao, "Navdreamer: Video models as zero-shot 3d navigators," *arXiv preprint arXiv:2602.09765*, 2026.